MOBSTER – II. Identification of rotationally variable A stars observed with *TESS* in sectors 1–4

J. Sikora,[1,2]★ A. David-Uraz ®,[3] S. Chowdhury,[4] D. M. Bowman,[5] G. A. Wade,[2]
V. Khalack,[6] O. Kobzar,[6] O. Kochukhov,[7] C. Neiner ®[8] and E. Paunzen ®[9]

[1]*Department of Physics, Engineering Physics & Astronomy, Queen's University, Kingston, ON K7L 3N6, Canada*
[2]*Department of Physics and Space Science, Royal Military College of Canada, PO Box 17000 Kingston, ON K7K 7B4, Canada*
[3]*Department of Physics and Astronomy, University of Delaware, Newark, DE 19716, USA*
[4]*Nicolaus Copernicus Astronomical Center, Bartycka 18, PL-00-716 Warsaw, Poland*
[5]*Instituut voor Sterrenkunde, KU Leuven, Celestijnenlaan 200D, B-3001 Leuven, Belgium*
[6]*Département de Physique et d'Astronomie, Université de Moncton, Moncton, NB E1A 3E9, Canada*
[7]*Department of Physics and Astronomy, Uppsala University, SE-751 20 Uppsala, Sweden*
[8]*LESIA, Paris Observatory, PSL University, CNRS, Sorbonne Université, Université de Paris, 5 place Jules Janssen, F-92195 Meudon, France*
[9]*Department of Theoretical Physics and Astrophysics, Masaryk University, KotlárŽská 2, CZ-611 37 Brno, Czech Republic*

ABSTRACT

Recently, high-precision optical 2-min cadence light curves obtained with *TESS* for targets located in the mission's defined first four sectors have been released. The majority of these high-cadence and high-precision measurements currently span ~ 28 d, thereby allowing periodic variability occurring on time-scales $\lesssim 14$ d to potentially be detected. Magnetic chemically peculiar (mCP) A-type stars are well known to exhibit rotationally modulated photometric variability that is produced by inhomogeneous chemical abundance distributions in their atmospheres. While mCP stars typically exhibit rotation periods that are significantly longer than those of non-mCP stars, both populations exhibit typical periods $\lesssim 10$ d; therefore, the early *TESS* releases are suitable for searching for rotational modulation of the light curves of both mCP and non-mCP stars. We present the results of our search for A-type stars that exhibit variability in their *TESS* light curves that is consistent with rotational modulation based on the first two data releases obtained from sectors 1 to 4. Our search yielded 134 high-probability candidate rotational variables – 60 of which have not been previously reported. Approximately half of these stars are identified in the literature as Ap (mCP) stars. Comparisons between the subsample of high-probability candidate rotationally variable Ap stars and the subsample of stars that are not identified as Ap reveal that the latter subsample exhibits statistically (i) shorter rotation periods and (ii) significantly lower photometric amplitudes.

Key words: stars: early-type – stars: magnetic field – stars: rotation.

1 INTRODUCTION

One fundamental property that distinguishes main sequence (MS) A-type stars with masses $1.5 < M < 3 \, \mathrm{M_\odot}$ from their lower mass ($M \lesssim 1.5 \, \mathrm{M_\odot}$) counterparts is the incidence rate of inhomogeneous surface brightness distributions, which are broadly referred to as star spots. Contrary to MS A-type stars, essentially all late-F, G-, and K-type MS stars exhibit bright and/or dim star spots (Cameron, Donati & Semel 2002; Berdyugina 2005; Ermolli et al. 2007). The relatively small fraction of MS A-type stars that do host qualitatively similar surface structures are known as α^2 CVn variables and are

identified based on detections of low-frequency photometric and spectroscopic variability (Samus' et al. 2017). While the origins of these surface structures differ, in both the spotted low-mass MS star and α^2 CVn cases, the observed photometric variability is understood to be a consequence of the star's rotation: the star's brightness is modulated as surface features appear and disappear from view.

It is well established that α^2 CVn variable stars are magnetic chemically peculiar (mCP) Ap stars (e.g. Babcock & Burd 1952). Furthermore, the origin of surface brightness inhomogeneities that lead to photometric rotational modulation in α^2 CVn stars can be traced to the presence of strong, organized magnetic fields that are visible at the stellar surface (Krtička et al. 2007, 2009, 2015). The mCP stars account for approximately 10 per cent of all MS A-type

★ E-mail: james.sikora@queensu.ca

stars with masses $\sim 3\,M_\odot$ (Wolff 1968; Aurière et al. 2007; Sikora et al. 2019b). They host strong, stable, and organized magnetic fields with strengths ~ 0.1–30 kG (Babcock 1960; Landstreet 1982). Recently, a small number of non-mCP MS A-type stars have been found to host ultra-weak (dubbed 'Vega-like' after the prototype of the population) fields with strengths $\lesssim 1$ G (Lignières et al. 2009; Petit et al. 2011; Blazère et al. 2016). It has been suggested that these stars may represent a new class of magnetic MS A-type stars that are distinct from the mCP stars (Lignières et al. 2014).

The *Kepler* (Borucki et al. 2010), K2 (Howell et al. 2014), and CoRoT (Auvergne et al. 2009) space-based photometry missions have resulted in the identification of a large number of MS A-type stars exhibiting variability that is consistent with rotational modulation (Balona 2011; Paunzen et al. 2015; Bowman et al. 2018). In particular, Balona (2013) reported the discovery that ~ 40 per cent of MS A-type stars observed with *Kepler* may exhibit photometric rotational variability. In addition to the rotational variables, Balona (2012, 2013) also identified (i) a number of apparently flaring A-type stars and (ii) unexplained periodogram features that are characterized by nearly coincident low-frequency diffuse and narrow peaks (e.g. fig. 6 of Balona 2013).

Pedersen et al. (2017) carried out a detailed analysis of 33 of the A-type stars that reportedly exhibit evidence of flares in their *Kepler* light curves. They confirmed the presence of flares in 27 of these stars' light curves but found that the flares associated with 14 of these cases may be attributed to contamination from nearby sources. Ultimately, these authors concluded that the flares identified by Balona (2012, 2013) are likely not intrinsic to the A stars themselves. In the case of the unexplained periodogram features, Balona (2014) suggested that the diffuse peaks may be caused by spots appearing on the surface of a differentially rotating A star while the narrow peaks are caused by close-in Jupiter-sized planets. However, Saio et al. (2018) argue for a more physically justified explanation in that the features in the amplitude spectra of many A stars are evidence of Rossby waves (also known as r modes, Papaloizou & Pringle 1978), which can occur in rotating γ Dor stars. Observational evidence of this phenomenon has been previously identified by Van Reeth, Tkachenko & Aerts (2016).

If the variability identified by Balona (2013) is indeed produced by spots on the surfaces of rotating A-type stars, then what is the origin of the spots? Such variability in these particular objects is normally attributed to the presence of magnetic fields that are visible at the surface. The reported ~ 40 per cent incidence rate of rotationally variable A-type stars is several times higher than the incidence rate of strongly magnetic (mCP) stars; therefore, it is unlikely that all of these stars are strongly magnetic. Considering that surface spots have been detected on Vega (which hosts an ultra-weak field, Böhm et al. 2015) and that such spots may lead to photometric variability, it is plausible that a large number of the A-type stars that were found to exhibit rotational modulation by Balona (2013) may host ultra-weak fields. Recently, Cantiello & Braithwaite (2019) explored the observational consequences of convection that might produce dynamo magnetic fields at or near the surfaces of fast-rotating A- and B-type stars. Referring to similar discussions presented by Cantiello & Braithwaite (2011) in the context of more massive stars, the authors note that such magnetic fields are expected to result in both ultra-weak fields and coincident spots characterized by low-temperature contrasts (~ 10 K) being present at the stellar surface. They predict that, while all A- and late B-type stars should host these features, they are likely largely undetectable. The fraction of stars for which the temperature spots can be expected to be detected depends on the size

and number of spots (Kochukhov & Sudnik 2013), which is not well constrained.

The MS A-type stars as defined in this study partly overlap with the mercury–manganese (HgMn) group of CP stars, which exhibit a distinct and unique rotational variability. HgMn stars have masses between $2.5\,M_\odot$ and $\sim 5\,M_\odot$ and effective temperatures as low as $10\,000$ K (Ghazaryan & Alecian 2016). These stars show no evidence of either global or strong complex magnetic fields (Aurière et al. 2010; Makaganiuk et al. 2010; Kochukhov et al. 2013), with the best upper limits on the longitudinal field component currently in the 1–10 G range. Nevertheless, many of these stars show rotational line profile variability indicative of low-contrast, large-scale inhomogeneous surface abundance distributions (Adelman et al. 2002; Kochukhov et al. 2005; Briquet et al. 2010; Folsom et al. 2010; Makaganiuk et al. 2012). Unlikely stationary spots on magnetic Ap stars, surface structures on HgMn stars evolve on time-scales from months to years (Kochukhov et al. 2007; Korhonen et al. 2013), suggesting a different underlying physical mechanism of their formation. A low-amplitude photometric modulation associated with chemical spots on HgMn stars is undetectable from the ground but can be identified using high-precision space photometric data (Alecian et al. 2009; Balona et al. 2011; Hodgson et al. 2017).

The MOBSTER collaboration (Magnetic OB[A] Stars with *TESS*: probing their Evolutionary and Rotational properties; David-Uraz et al. 2019) is focused on advancing our understanding of stellar magnetism of intermediate- and high-mass stars using *TESS* observations along with spectroscopic and spectropolarimetric follow-up observations. The primary goal of the study presented here, which is the second of a series of publications by the MOBSTER collaboration, is to identify new candidate rotational variable MS A-type stars based on the release of *TESS* observations. These stars are hypothesized to host either strong magnetic fields (similar to those associated with mCP stars) or ultra-weak fields (similar to that found on Vega, Lignières et al. 2009). Since these stars are generally much brighter than those detected by *Kepler*, these identifications will serve as the basis for spectropolarimetric surveys designed to detect such magnetic fields, as was proven a successful strategy with stars observed by K2 (e.g. Buysschaert et al. 2018).

In Section 2, we describe the *TESS* observations on which our study is based. In Section 3, we describe our sample of A-type stars and the methods by which it was constructed. In Section 4 ,we discuss how our search for rotationally modulated *TESS* light curves was carried out and present the results of this search. In Section 5, we present the fundamental parameters (i.e. effective temperatures, radii, masses, etc.) associated with our sample and describe the way in which they were derived. In Section 6, we discuss some of the more noteworthy targets identified as candidate rotational variables. Finally, in Section 7, we summarize and discuss the results of this study.

2 OBSERVATIONS

TESS is optimized to detect planetary transit signatures in light curves of MS dwarf stars having I_C magnitudes of approximately $4-13$ (Ricker et al. 2015). For typical MS A-type stars, which are the focus of this study, the I_C limits correspond to Johnson *V* magnitudes of approximately $3-12$. The passband of the filter used by the onboard photometer has an effective wavelength of ≈ 7500 Å and a width of ≈ 4000 Å (Sullivan et al. 2015). In this study, we used the 2-min PDC_SAP light curves processed by the *TESS* Science Team. These light curves are available from the Mikulski Archive

for Space Telescopes (MAST).[1] We refer the reader to Jenkins et al. (2016) for a description of the pipeline that produces these light curves.

The *TESS* data considered in this study consist of targets located in sectors 1–4. These sectors are in the southern ecliptic and contain targets with right ascension (RA) values of RA $< 131°$ and RA $> 308°$ and declination (Dec) values of $-85 <$ Dec $< +12°$. The observations have been obtained over a period of ≈ 4 months from July 25 to November 14, 2018. Sectors 1 and 2, sectors 2 and 3, and sectors 3 and 4 partially overlap where Dec $\lesssim -30°$; the light curves associated with the targets found in only one sector (the majority of the targets) span 28 d while those associated with targets found in two sectors span 56 d. The brightness measurements exhibit typical uncertainties of $\lesssim 800$ parts per million (ppm).

3 SAMPLE

TESS light curves of 44 371 targets in sectors 1–4 were made available during the first two data releases. In order to identify the A-type stars within this sample, we first cross-referenced this list with the SIMBAD astronomical database[2] for available spectral types associated with those targets. No spectral types could be found for 20 098 of the 44 371 observed targets while a further 5 083 targets could not be found within SIMBAD. We identified 1 715 A-type stars from the 19 190 *TESS* targets with available spectral types.

We attempted to identify the A-type stars in the subset of 25 181 stars (20 098 + 5 083) without available spectral types using their effective temperatures ($T_{\rm eff}$). The *TESS* Input Catalogue (TIC, Stassun et al. 2018) includes $T_{\rm eff}$ values that are either derived from $(V - K_{\rm S}) - T_{\rm eff}$ calibrations (Casagrande, Flynn & Bessell 2008; Huang et al. 2015) or are taken from published spectroscopic surveys. Typical A-type stars exhibit $7\,000 \lesssim T_{\rm eff} \lesssim 10\,000$ K; however, the colour–$T_{\rm eff}$ calibrations used for the majority of the $T_{\rm eff}$ values reported in the TIC are only applicable to stars having $T_{\rm eff} \leq 9\,755$ K. Out of the subset of 25 181 observed stars without available spectral types that are listed in the TIC, 228 exhibit $7\,000 \leq T_{\rm eff} \leq 9\,755$ K and another 228 have not been assigned $T_{\rm eff}$ values (i.e. their $T_{\rm eff}$ values could not be estimated using the $(V - K_{\rm S}) - T_{\rm eff}$ calibrations and no spectroscopically determined $T_{\rm eff}$ values are available).

Johnson *B* and *V* magnitudes are available for 93 of the 228 stars without $T_{\rm eff}$ values listed in the TIC. We estimated their $T_{\rm eff}$ values using the $(B - V) - T_{\rm eff}$ calibration published by Gray (2005) for MS stars. This colour–$T_{\rm eff}$ calibration is reasonably sensitive to stars with $T_{\rm eff} \lesssim 10\,000$ K; the scatter associated with the calibration is estimated to be ≈ 2–5 per cent. The $(B - V) - T_{\rm eff}$ calibration yielded 19 stars having $7000 \leq T_{\rm eff} \leq 10\,000$ K and are therefore considered to be candidate A-type stars.

In summary, out of the 44 371 targets included in the first two *TESS* data releases, we identified a total of 1 962 A-type stars based on (i) published spectral types (1 715 stars), (ii) the $(V - K_{\rm S}) - T_{\rm eff}$ calibrations used in the TIC (228 stars), and (iii) $(B - V) - T_{\rm eff}$ calibrations (19 stars). We note that by adopting a minimum $T_{\rm eff}$ value of 7000 K in our search for A-type stars within the subsample of those stars without available spectral types, a number of cooler A-type stars will likely have been missed. While this is unlikely to significantly impact the broader findings of our study, it may have

an impact on the results associated with the coolest and lowest mass A-type stars in our sample.

Johnson *V* magnitudes for all but one of the 1962 A-type stars included in our sample are listed in the TIC. The sample exhibits a median *V* magnitude of 8.7 mag and ranges from 16.4 to 2.9 mag. Distances (*d*) derived from the parallax angles associated with the second Gaia Data Release (DR2) (Gaia Collaboration et al. 2016; Bailer-Jones et al. 2018; Holl et al. 2018) for 1906 of the 1962 sample stars are available; based on these values, the majority of the stars in the sample are relatively nearby with 90 per cent having $d \lesssim 440$ pc. Out of the 1962 stars in our sample, 363 are located in overlapping sectors and thus, their light curves have a temporal baseline of 56 d while the remaining 1599 appear only in one sector and have temporal baselines of 28 d.

4 ROTATIONAL MODULATION

4.1 Search criteria

We carried out a search for rotationally modulated variability in the set of *TESS* light curves by adopting the main criteria outlined by Balona (2011, 2013): (i) the frequency spectrum of the light curve (i.e. the periodogram) must exhibit a low-frequency peak ($f_1 \lesssim 3\,{\rm d}^{-1}$) that plausibly corresponds to the star's rotational frequency and (ii) this peak must be accompanied by a first harmonic ($f_2 = 2f_1$). The first criterion is based on the fact that the critical rotation frequency of a zero age MS (ZAMS) A-type star ranges from $f_{\rm crit} \approx 3 - 3.7\,{\rm d}^{-1}$. As described by Balona (2013), the second criterion is adopted as a means of minimizing the number of stars exhibiting low-frequency signals that may be caused by pulsations rather than rotational modulation (e.g. γ Dor stars and slowly pulsating B-type stars, Cousins, Caldwell & Menzies 1989; Waelkens 1991; De Cat & Aerts 2002; Henry & Fekel 2003).

As a result of the second criterion, rotational variables may not be detected in our study if the amplitude of the first harmonic (A_2) is low. The ratio of the amplitude of the rotational frequency (A_1) to A_2 depends largely on the distribution of co-rotating surface structures (i.e. spots) and on the inclination angle, *i*, of the star's rotational axis. We attempted to evaluate the selection effect that the second criterion has on our sample of identified rotational variables by using the analytical spot model developed by Eker (1994). The model consists of a rigidly rotating star having one or more circular surface spots positioned at various longitudes and latitudes. The inclination of the star's rotation axis, the manner in which limb darkening is treated (i.e. whether it is neglected or described by a linear or quadratic limb darkening law), and the spot radii and contrast values are input parameters that can be modified in this model.

The expected range of the ratio A_1/A_2 was estimated by carrying out several Monte Carlo (MC) simulations. We generated 500 models each for cases in which between one and five spots are present on the star's surface. For each model, the star's *i* value, spot longitudes, latitudes, and angular radii (ranging from 2 to 30°) were randomly assigned; for those models with more than one spot, the same radius was adopted for each spot. We used a linear limb darkening law with a coefficient of $u = 0.589$, which is computed by Díaz-Cordovés, Claret & Gimenez (1995) in the *V* band for a 7000 K star with $\log g = 4.0$ (cgs). We adopted a rotation period of 2.5 d and the light curves were then calculated during 40 d (16 rotational cycles) with a cadence of 2 min. Lomb–Scargle (LS) periodograms (Lomb 1976; Scargle 1982; Press 2007) were calculated for each synthetic light curve (the same technique
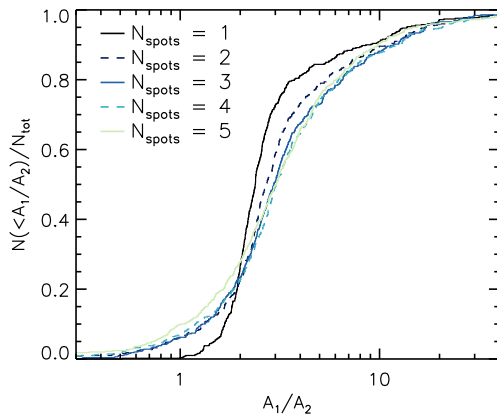

Figure 1. Cumulative distribution functions corresponding to A_1/A_2 based on the spot model published by Eker ([1994](#)). The distributions for models with 1, 2, 3, 4, and 5 spots are shown increasing in brightness from dark blue to light blue and alternating between solid and dashed lines.

was employed in the analysis of the *TESS* light curves, as described below) from which the values of A_1 and A_2 were extracted in units of magnitude.

In Fig. [1](#), we show the cumulative distribution functions for A_1/A_2 associated with the MC simulations carried out with one to five. The results suggest that stars having multiple spots are more likely to exhibit A_1/A_2 ratios that are $\gtrsim 2$ compared to stars with single spots. This implies that stars with complex spot distributions are less likely to satisfy the second criterion in our search for rotational modulation since, depending on the value of A_1, the value of A_2 is more likely to fall below the detection threshold. It is also noted that a non-negligible fraction ($\sim$10 per cent) of the models exhibiting more than one spot have $A_1/A_2 < 1$ and thus, the rotation frequency does not necessarily correspond to the periodogram peak with the largest amplitude.

The two criteria used to identify rotationally modulated light curves are also frequently satisfied by eclipsing binaries (EBs) and ellipsoidal variables (EVs). EBs are easily identified based on the presence of primary and secondary eclipses in their light curves; however, EVs can exhibit highly sinusoidal light curves similar to those produced by rotational modulation (e.g. fig. [10](#) of Smalley et al. [2014](#)). In order to reduce the number of EVs misclassified as rotational variables, we rejected any non-Ap rotational variable candidates with light curves exhibiting a deep local minimum followed by a shallower local minimum that are both bracketed by the system's maximum brightness. These characteristic features of EVs are often easy to identify when the light curve is phased by the system's orbital period since the two minima have a phase separation of 0.5. Furthermore, the distances separating the two components of an EV system are relatively low and the inclination of the orbital plane is relatively high; therefore, radial velocity variations are often large and easy to detect (e.g. Matson et al. [2017](#)). We searched the literature for any reported detections of radial velocity variations from which orbital periods have been derived. Those candidate rotational variables with reported orbital periods consistent with the photometric periods that were originally attributed to the star's rotation were rejected.

The last step of the search process involved classifying the identified candidate rotational variables as either low- or high-probability candidates. In a number of cases, the rotation and first harmonic peaks were accompanied by additional low-frequency

peaks with comparable amplitudes (e.g. γ Dor stars, Henry & Fekel [2003](#)). These stars were considered to be low-probability candidate rotational variables due to our inability to distinguish between those peaks that are caused by rotational modulation and those which are caused by pulsations; all other candidates were assigned a high-probability status.

4.2 Application of the search criteria to the *TESS* sample

We found that the signatures of rotational modulation in the light curves that were reduced and made publicly available by the *TESS* team could be more clearly identified after they were post-processed. This involved manually removing obvious outliers and detrending instrumental systematics by subtracting a low-order polynomial. We note that this detrending process may remove long-term trends described by periods that are approximately one or more times as long as the total light curve's timespan. First- or second-order polynomial fits are unlikely to remove short-period signals that are strictly periodic; however, signals that exhibit variations between consecutive cycles (e.g. such as those which might be associated with evolving star spots) are more susceptible to being removed.

We calculated LS periodograms of these post-processed light curves using an oversampling factor of 10 to ensure that peaks in a periodogram were well resolved. Statistically significant peaks were then identified using an iterative pre-whitening procedure similar to that described by Morel et al. ([2011](#)). For each iteration, the frequency of the maximum-amplitude peak (f_{max}) appearing in the periodogram was identified and a first-order sinusoidal function having frequency f_{max} (i.e. $A \sin[2\pi f_{max} t + \phi]$ where A, t, and ϕ correspond to the semi-amplitude, time, and phase) was fit to the light curve with A and ϕ as free parameters. The fit was then subtracted from the light curve and the LS periodogram was recalculated. This procedure was repeated until either 50 frequencies had been extracted or until no peaks having a statistical significance $\geq 5\sigma$ were found (the significance is evaluated according to equation (13.8.7) of Press [2007](#)). Uncertainties in all the extracted frequencies and their associated amplitudes were estimated using the prescriptions described by Montgomery & O'Donoghue ([1999](#)), which involve the root-mean-square deviation (RMSD) of the noise inherent in the light curve ($\sigma[m]$). We estimated $\sigma(m)$ by taking the RMSD of the light curve once all of the statistically significant signals had been removed.

After extracting the frequencies as described above, we carried out an automated routine designed to identify rotation (f_1) and first harmonic (f_2) frequency pairs. The first harmonic is given by $f_2 = 2f_1 \pm \Delta f$ where Δf is defined as the half-width at half-maximum of the central peak of each light curve's spectral window function corresponding to a typical value of $0.02\,\mathrm{d}^{-1}$. The 1695 light curves exhibiting low-frequency peaks with accompanying first harmonics were then inspected visually; those targets with obvious EB, EV, or pulsational (e.g. RR Lyrae stars) signatures were removed from the list of candidate rotational variables. The remaining candidates were then assigned either a low-probability or high-probability candidate rotational variable classification based on the appearance of additional low-frequency, high-amplitude peaks (described in Section 4.1).

Having identified periodogram peaks that are likely associated with each star's rotation period ($P_{rot} = 1/f_1$), we refined the final P_{rot} values using a Levenberg–Marquardt least-squares algorithm. This involved fitting the light curves to a sinusoidal function that

Table 1. Parameters associated with the 134 identified high-probability candidate rotational variables. Columns (1)–(8) list the TIC identifiers, alternative identifiers, spectral types, V magnitudes, maximum photometric amplitudes associated with the rotational modulation signals (ΔT_{max} where the 1 or 2 subscript indicates whether ΔT_{max} corresponds to f_1 or f_2), rotation periods inferred from the *TESS* light curves, published rotation periods, and notes. The numbers in parentheses in rotation periods indicate the uncertainty in the value (3σ uncertainties are listed for both ΔT_{max} and P_{rot}). We note the confidence with which any reported magnetic field measurements in the literature have been obtained: definite detections (DD), marginal detections (MD), and null detections (ND). Additionally, we note whether each star is identified as a spectroscopic binary (SB), visual binary (VB), δ Scuti pulsator, roAp star, and if the amplitude of the rotational modulation is found to vary over time (amplitude modulation, AMod). Those stars without $P_{rot, pub}$ values are considered new rotational variables; similarly, those δ Scuti and roAp identifications that are not accompanied with references are considered new classifications. The full table appears only in the electronic version of the paper.

TIC	Alt. ID	Sp. Type	V (mag)	ΔT_{max} (mmag)	P_{rot} (d)	$P_{rot, pub}$ (d)	Notes
(1)	(2)	(3)	(4)	(5)	(6)	(7)	(8)
7624182	HD 27342	A2/3V	8.8	0.62(2)[1]	1.720(1)		
7780491	HD 28430	ApEuCrSr	8.2	3.50(2)[2]	1.8763(3)		
10863314	HD 10653	A1IV	7.7	2.06(2)[2]	2.1345(6)		
12359289	HD 225119	ApSi	8.2	5.14(3)[2]	3.0644(5)	2.944[a], 3.06395(41)[b]	
12393823	HD 225264	A0IV	8.3	0.83(1)[1]	1.4237(6)	1.42353(23)[b]	SB[+ c] ND[d]
24186142	HD 5601	ApSi	7.6	2.47(3)[1]	9.85(2)	1.110[e]	DD[f]
24225890	HD 5823	ApSrEu(Cr)	10.0	6.88(6)[2]	5.007(3)	1.245[e]	
27985664	HD 3885	ApSi	9.8	11.99(9)[2]	1.8144(3)	1.815[e]	
29432990	HD 198966	A9V	9.2	0.11(2)[1]	1.267(3)		
29666185	HD 199917	A2III/IV	7.1	0.50(1)[1]	1.0594(5)		AMod
29755072	HD 200299	A3III	7.7	0.97(1)[2]	6.180(4)		
29781099	HD 27997	A2mA5-A9	8.1	0.392(7)[2]	2.8749(9)		
32035258	HD 24188	ApSi	6.3	11.40(2)[1]	2.2303(1)	2.230[e], 2.23047(4)[b]	DD[d]
38586082	HD 27463	ApEuCr(Sr)	6.3	12.59(3)[1]	2.8349(2)	2.835750[g], 2.8349(1)[b]	δ Scuti[b]
41259805	HD 43226	ApSr(Eu)	9.0	11.23(3)[1]	1.71450(4)	1.714[e], 1.71441(11)[b]	roAp[h]
42055368	HD 10038	A2mA5-F0	8.1	3.18(2)[2]	2.3120(4)		
44627561	HD 215559	A7V	9.3	21.1(1)[1]	3.1284(6)	1.563140[g]	δ Scuti, AMod
44678216	HD 25267	ApSi	4.6	7.5(2)[1]	3.861(4)	1.210[e]	DD[i]
44889961	HD 26726	ApSr	9.8	18.66(3)[1]	5.3818(9)	5.382[e]	
52368859	HD 10081	ApSr(Eu)	9.6	9.47(4)[2]	1.57052(9)	1.570[e], 1.57056(6)[b]	AMod

Note: +: $P_{orb} = 5.400945(40)$ d
[a] Catalano et al. (1998), [b] Cunha et al. 2019 (submitted), [c] Pourbaix et al. (2004), [d] Bagnulo et al. (2015)
[e] Netopil et al. (2017), [f] Kudryavtsev et al. (2006), [g] Oelkers et al. (2018), [h] Borra & Landstreet (1980)

includes the first four harmonics:

$$\Delta T(t) = a_0 + \sum_{n=1}^{n=5} a_n \sin\left(2\pi nt/P + \phi_n\right), \qquad (1)$$

where a_0, a_n, ϕ_n, and P are free parameters. The a_1 and P parameters are assigned initial guesses of half the range of $\Delta T(t)$ and $1/f_1$, respectively, while all other parameters are assigned initial guesses of zero. The uncertainties in each of the fitting parameters were estimated using a residual bootstrapping method. The refined rotation periods associated with the high-probability candidates along with the maximum amplitudes (ΔT_{max}, i.e. the largest a_n, which always corresponds to either a_1 or a_2) associated with the sinusoidal fitting function are listed in Table 1.

In Fig. 2, we show sample light curves and their associated periodograms of several Ap stars identified as high-probability candidate rotational variables. Similarly, Fig. 3 shows examples of stars that are classified as non-chemically peculiar (i.e. their spectral types do not contain a 'p' classification) in the literature and are also considered to be high-probability candidate rotational variables. The search yielded 134 high-probability and 126 low-probability candidate rotational variables, respectively. This corresponds to an incidence rate of 6.8 ± 0.6 per cent. Including those stars identified as low-probability rotational variables increases this incidence rate to 13.3 ± 0.9 per cent. Out of the 134 high-probability candidate rotational variables, 76 are classified as Ap stars, 3 are classified as Am stars, 7 have luminosity classes of II or III (i.e. they have likely

evolved off the MS), and 48 are either classified as non-chemically peculiar MS stars or are unclassified.

The distribution of the inferred rotation periods of the 134 high-probability rotational variables is shown in Fig. 4. The longest period is ≈ 20 d; 81 per cent of the 134 stars exhibit $P_{rot} < 5$ d. Statistically, chemically peculiar Ap stars are known to have significantly longer rotation periods compared with their chemically normal, main sequence counterparts (e.g. Wolff 1975; Abt & Morrell 1995). Comparing the high-probability candidate rotational variables with Ap classifications with the remainder of the high-probability candidates, we find that the Ap stars have statistically longer inferred P_{rot} values: this is apparent from the cumulative distribution functions shown in the inset plot of Fig. 4. We also compare the rotation periods of the 76 Ap stars with those of the sample of nearby magnetic Ap stars studied by Sikora et al. (2019a). The *TESS* light curves span a period range of ≈ 30 d for the majority of the stars in our sample (i.e. for those stars that are found in only one sector), which implies that only rotation periods of $P_{rot} \lesssim 15$ d can be detected. Comparing the distributions of those stars in the two samples having $P_{rot} < 15$ d – 75/76 of the Ap stars included in this study and 43/48 of the stars included in the survey carried out by Sikora et al. (2019a) – yields close agreement.

In Fig. 5, we show the distribution of maximum *TESS* photometric amplitudes (ΔT_{max}, i.e. the maximum of the amplitudes associated with f_1 and f_2) for the identified 134 high-probability rotational variables. The distribution ranges from 3 to 52 mmag and exhibits
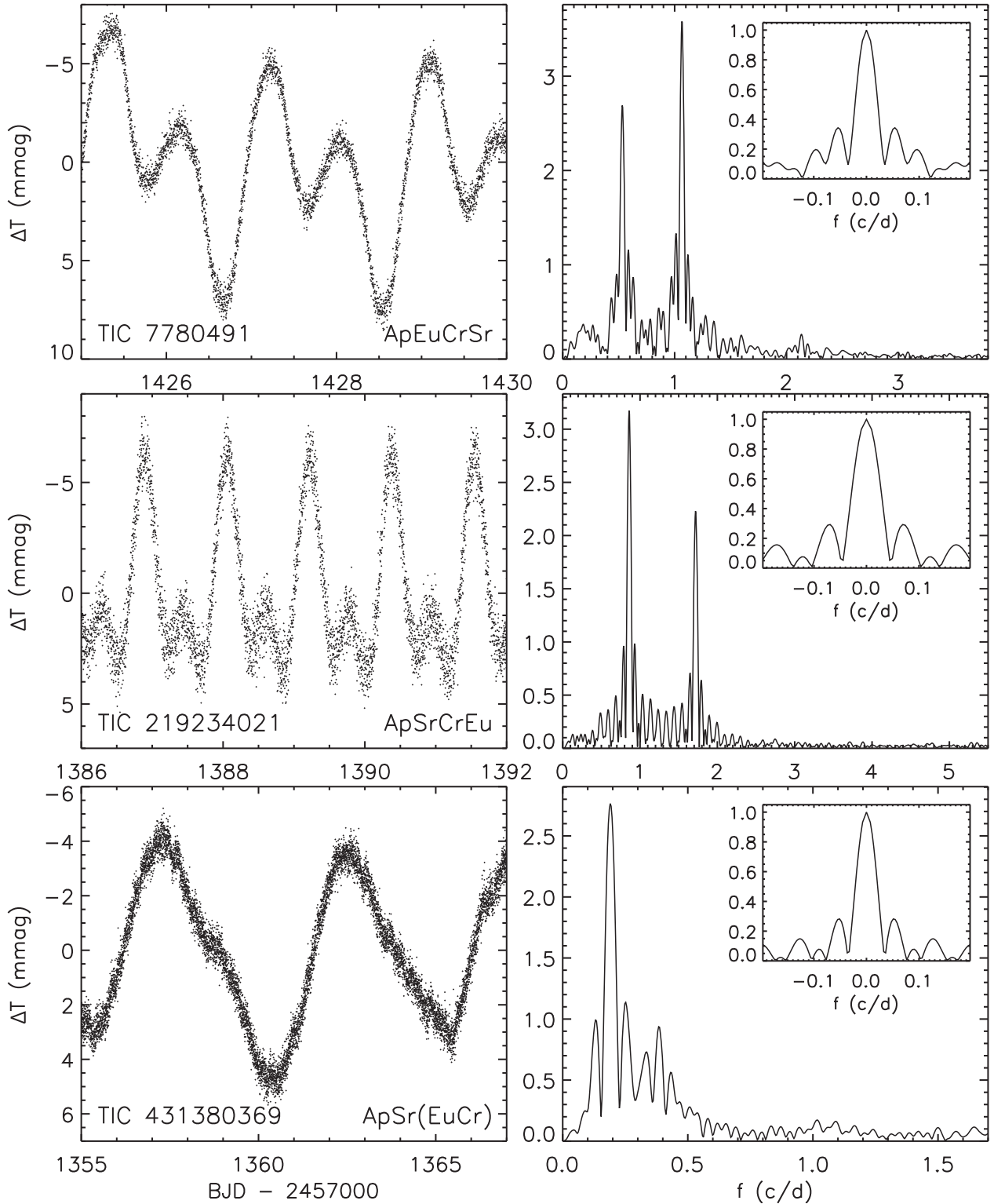
Figure 2. Examples of *TESS* light curves associated with Ap stars that are found to exhibit variability that is consistent with a rotational origin. *Left:* Subsamples of the full light curves. *Right:* The Lomb–Scargle periodograms derived from the light curves. The rotational frequencies believed to be the stars' rotational frequencies are apparent along with the first harmonic. The spectral window function is shown in the inset at upper right.

a median value ∼6 mmag. Comparing the distributions of ΔT_{max} associated with the Ap stars and those not identified as Ap, it is evident that the sample of Ap stars tends to exhibit larger ΔT_{max} values.

We searched the light curves of the identified 134 high-probability candidate rotational variables for evidence of amplitude modulation (AMod). This was carried out by dividing each light curve into sections spanning one rotational cycle (defined by P_{rot}); those
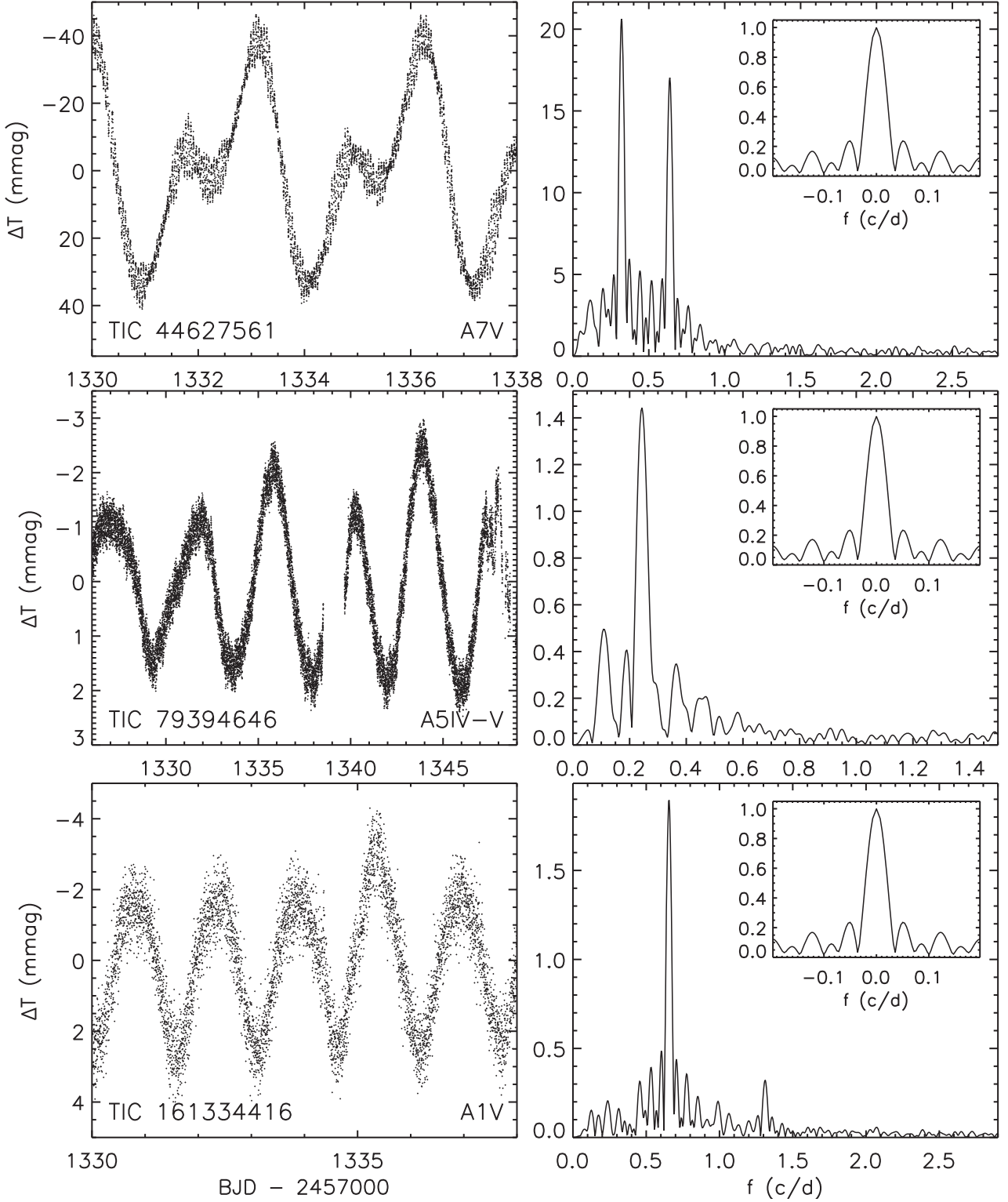
Figure 3. Same as Fig. 2 but for non-Ap stars. Note that TIC 44627561 (top) exhibits high-frequency ~20 d^{-1} variability that is typical of δ Scuti stars.

sections having a coverage $\lesssim 80$ per cent of the rotational cycle were discarded. The sections were then individually fit using equation (1) with P fixed at $P_{\rm rot}$ while allowing the a_n and ϕ_n terms to vary. Evidence of AMod is manifest as changes in the amplitudes associated with the rotation frequency and first four harmonics (a_n where n goes from 1 to 5) over time. In many cases,

the variations in a_n were found to be correlated with the level of noise throughout the light curve; those sections of the light curve that were obviously affected by the level of noise were disregarded. We identified 22 instances of clear AMod that is not obviously induced by changes in the noise level or by the detrending process that was applied to the light curves. These cases are noted in Table 1;
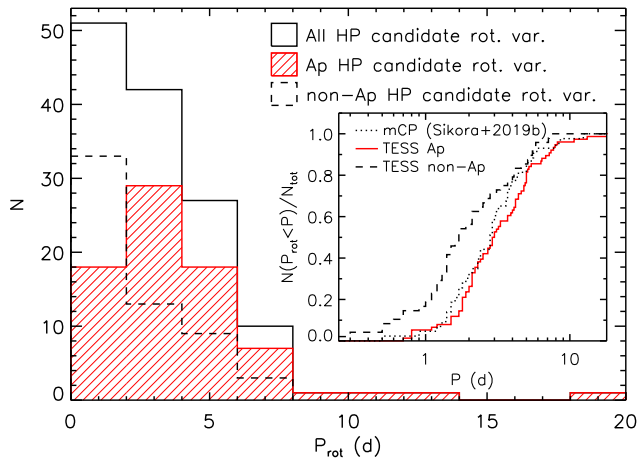
Figure 4. Distributions of the rotation periods (P_{rot}) obtained from the *TESS* light curves associated with the high-probability (HP) rotational variable candidates for the total sample (solid black), subsample of Ap stars (red hatched), and subsample of non-Ap stars (dashed black). *Inset:* The cumulative distribution functions associated with the P_{rot} values of the *TESS* stars not classified as being Ap (dashed black), the *TESS* stars classified as Ap (solid red), and the confirmed mCP stars having $P_{rot} < 15$ d (90 per cent of the sample of mCP stars) included in the survey carried out by Sikora et al. (2019a) (dotted black).
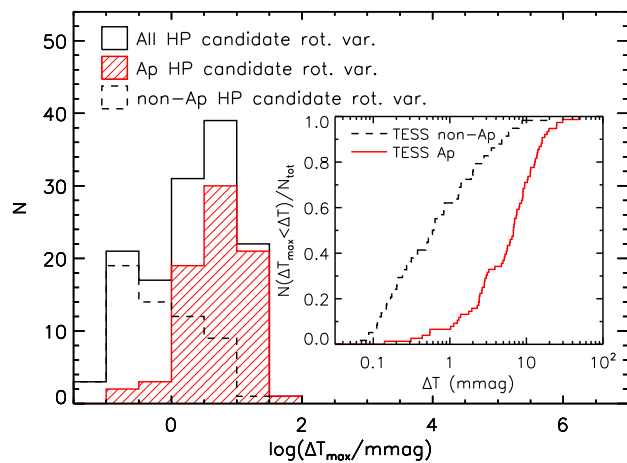
Figure 5. Distributions of the maximum photometric amplitudes (ΔT_{max}) associated with the rotational modulation for the high-probable (HP) rotational variable stars: the total sample (solid black), subsample of Ap stars (red hatched), and subsample of non-Ap stars (dashed black) are shown. The cumulative distribution functions associated with the non-Ap (dashed black) and Ap (solid red) are shown in the inset plot.

examples of such light curves are shown in Fig. 6. In several of the light curves, the detected AMod could have a beating effect caused by low-amplitude (pulsation) frequencies in a narrow frequency near the rotation frequency (e.g. Degroote et al. 2011; Bowman et al. 2016) produced by pairs of signals having narrow frequency spacings. An example of this is shown in the second panel of Fig. 6 (TIC 70525154). The apparent beating could also be induced by the presence of binary companions or background variable stars; therefore, the detected AMod may not be intrinsic to the A stars themselves. Out of the 22 stars, 3 have likely evolved off of the MS based on their luminosity classes of II or III, 1 is an Am star, 8 are Ap stars, and 10 are not identified as chemically peculiar. The

inferred rotation periods of the three evolved stars and 1 Am star are all < 1 d while those of the 8 Ap stars and remaining 10 non-Ap stars are between 0.5 and 4.4 d.

The study recently carried out by Cunha et al. (submitted) focuses on Ap stars observed with *TESS* in sectors 1 and 2. It consists of 83 stars located in sectors 1 and 2; they find that 61 of these targets exhibit variability that is consistent with rotational modulation and for which rotation periods could be inferred from the *TESS* light curves. A total of 76 out of the 83 stars in their sample are also found in our sample while the 7 stars that are excluded have reported spectral types of either F or B and thus were filtered out during the construction of our sample. The majority of our identifications of candidate rotational variables is in agreement with those reported by Cunha et al. (submitted): only four stars that these authors identify as rotational variables are not identified as such in our survey due to the difficulty with which we were able to identify clear rotation and first harmonic frequency pairs in accordance with the search criteria outlined in Section 4.1. For example, TIC 394124612 exhibits a large number of low-frequency peaks in the periodogram associated with its light curve; as a result, we could not definitively attribute a single peak to the star's rotation frequency.

5 FUNDAMENTAL PARAMETERS

The TIC (Stassun et al. 2018) provides a number of fundamental stellar parameters including effective temperatures, luminosities, radii, and masses. For 12 of the 1962 stars in the sample of A-type stars, the reported fundamental parameters are obtained from large spectroscopic surveys that have been compiled into the TIC. For the majority of the stars (1900 of the 1962 stars in the sample), the fundamental parameters listed in the TIC have been derived using the $(V - K_S) - T_{eff}$ calibration published by Huang et al. (2015). Comparisons between the extracted spectral types of the stars in our sample with the T_{eff} values derived from this colour–T_{eff} calibration suggest that many of the temperatures may be inaccurate (e.g. TIC 13373403 is an A0/1V star with a reported $T_{eff} = 5500$ K and TIC 30728476 is an A7V star with a reported $T_{eff} = 9200$ K). As a result, we decided to derive the fundamental parameters for our sample using several methods.

5.1 SED fitting

We derived temperatures, luminosities, and stellar radii by fitting the available photometric observations with synthetic spectral energy distributions (SEDs). The TIC contains Johnson B and V magnitudes for 1956 of the 1962 A-type stars in our sample and 2MASS J, H, and K_S (Cohen, Wheaton & Megeath 2003) magnitudes for 1959 stars. We searched additional catalogues for available Johnson U (31 stars, Ducati 2002), Tycho B_T and V_T (953 stars, ESA 1997), Strömgren *uvby* (537 stars, Hauck & Mermilliod 1997), and Geneva $UB_1BB_2VV_1G$ (402 stars, Rufener & Nicolet 1988) magnitudes. All of the photometric measurements were converted from magnitudes to physical flux units using published Johnson, Tycho (Bessell & Murphy 2012), Strömgren (Bessell 2011), Geneva (Rufener & Nicolet 1988), and 2MASS (Cohen et al. 2003) zero points.

Colour excess values ($E[B - V]$) associated with 1885 and 1457 of the 1962 stars in our sample are listed in the TIC and reported by Gontcharov & Mosenkov (2017), respectively. We found that de-reddening the flux measurements using the values taken from either of these catalogues prior to carrying out the SED fitting analysis yielded a large number of T_{eff} values that are significantly greater than is expected for A-type stars ($T_{eff} > 12\,000$ K). Furthermore,
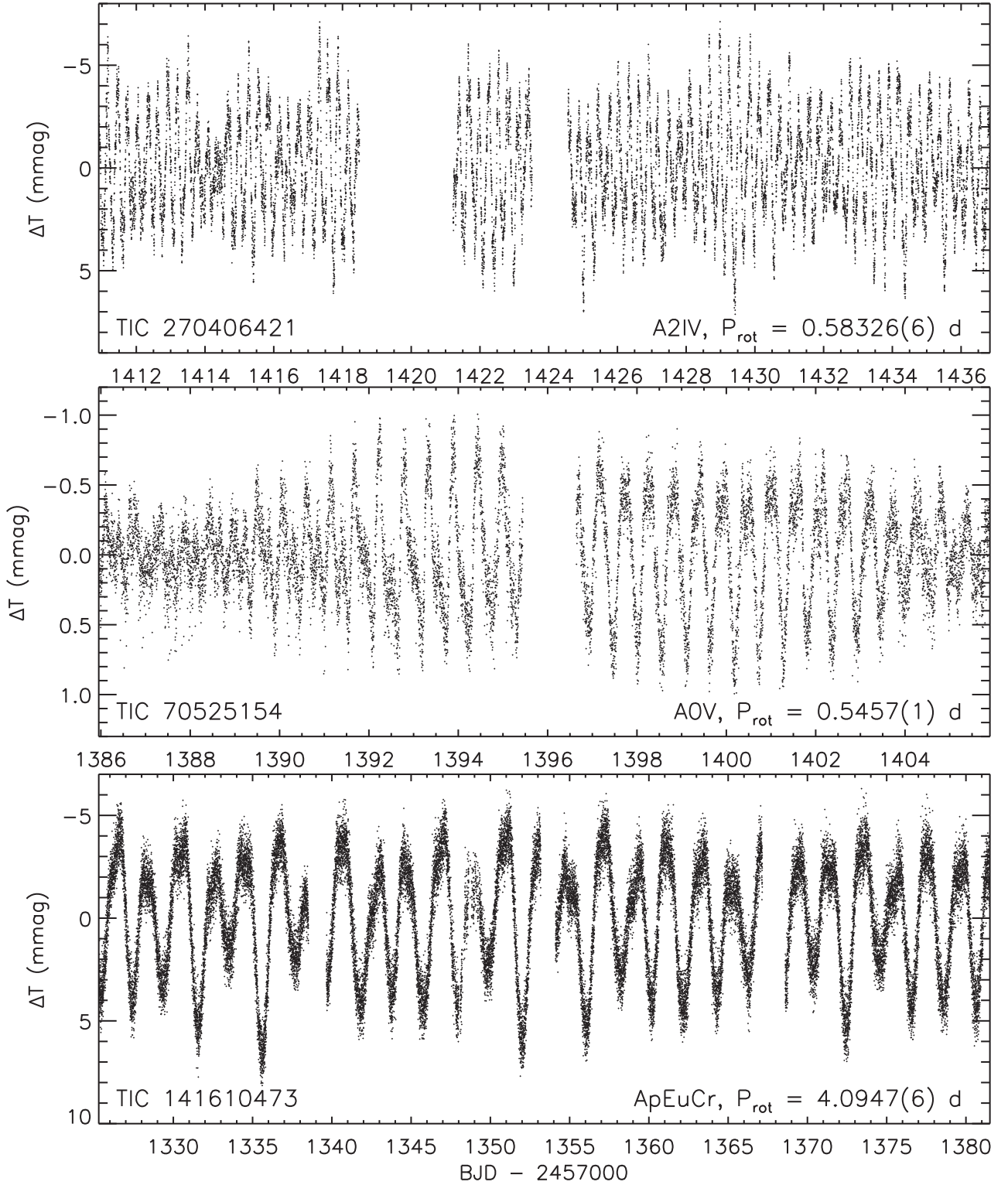
Figure 6. Examples of *TESS* light curves exhibiting rotational modulation with variable amplitudes (amplitude modulation, AMod).

based on the distances derived from the Gaia DR2 parallax measurements (Bailer-Jones et al. 2018), many of these stars were found to be positioned well below the main sequence in the Hertzsprung–Russell Diagram. As a result, we opted to derive the fundamental parameters with $E(B - V) \equiv 0$.

We used the grid of synthetic SEDs published by Castelli & Kurucz (2003) to fit the photometric observations. The grid consists of models having $5\,000 \leq T_{\mathrm{eff}} \leq 20\,000$ K in increments of $250 - 1000$ K, surface gravities of $3 \leq \log g \leq 5$ (cgs) in increments of 0.5, and metallicities of $-2.5 \leq [M/H] \leq +0.5$ in
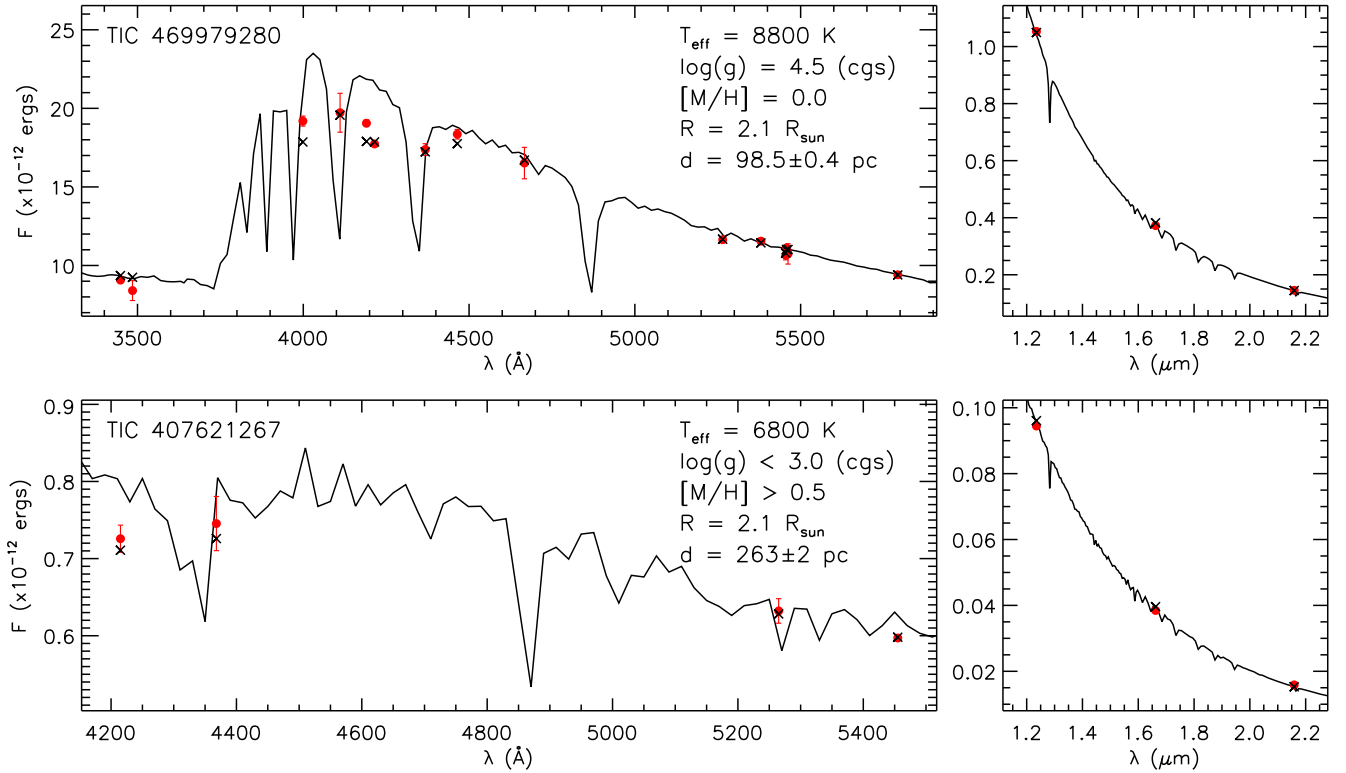
Figure 7. Two examples of the fits yielded by the SED fitting analysis involving various photometric filters. The filled red circles correspond to the observed flux measurements; the black 'X' symbols correspond to the model flux associated with the various filters. *Top:* Fit obtained with Johnson, Tycho, Strömgren, Geneva, and 2MASS filters. *Bottom:* Fit obtained with Johnson, Tycho, and 2MASS filters.

increments of $0.2-0.5$. The model SEDs are computed using the solar abundances published by Grevesse & Sauval ([1998](#)). The model flux associated with each photometric filter was then computed using the transmission functions obtained from the same publications from which the zero points were obtained. The grid of synthetic SEDs was linearly interpolated in T_{eff}, $\log g$, and $[M/H]$ in order to produce a uniform grid having $\Delta T_{eff} = 50$ K, $\Delta \log g = 0.5$, and $\Delta [M/H] = 0.5$.

The best-fitting T_{eff}, $\log g$, and $[M/H]$ were derived using a grid-search χ^2 minimization analysis that was carried out with the interpolated grid of models. The χ^2 value associated with each grid point was calculated after deriving an angular radius ($\alpha \equiv (R/d)$, where R and d correspond to the star's radius and distance, respectively); for those stars with known distances, the angular radius was used to infer the stellar radii. The distances were primarily obtained from Bailer-Jones et al. ([2018](#)), which are based on Gaia DR2 parallax measurements (1906 of 1962 stars in the sample). Additional distances were obtained from the Gaia DR1 parallax measurements derived by Astraatmadja & Bailer-Jones ([2016](#)) (9 of 1962 stars), Hipparcos parallax measurements (van Leeuwen [2007](#)) (28 of 1 962 stars), or Tycho parallax measurements (ESA [1997](#)) (2 of 1962 stars); no distances could be obtained for 17 of 1962 stars. For 88 stars, $[M/H]$ values are listed in the TIC; in these cases, $[M/H]$ was fixed at the reported values. The T_{eff} and R values were used to derive the luminosities (L) of the stars in our sample based on the Stefan–Boltzmann relation. In Fig. [7](#), we show two examples of the obtained fits to the observed photometry. The uncertainties in T_{eff}, $\log g$, $[M/H]$, R, and L were estimated using the residual bootstrapping method described by Sikora et al. ([2019b](#)); note that the uncertainties in R and L include

the errors in the distances that are propagated through the scaling factor α.

Effective temperatures were derived for 1913 stars through the SED fitting analysis. Based on our bootstrapping method of estimating uncertainties, we find that 1765 of these stars (92 per cent) exhibit $\sigma_{T_{eff}} \leq 200$ K. For nearly all of those stars that were found to have $\sigma_{T_{eff}} \geq 400$ K, only Johnson B and V and 2MASS J, H, and K_S measurements are available (only two of the stars with more than five available measurements were found to have $\sigma_{T_{eff}} \geq 400$ K). Overall, only moderate differences are evident between those $\sigma_{T_{eff}}$ values obtained from stars with only five available measurements compared to those with more than five: we find that $\langle \sigma_{T_{eff}} \rangle = 150$ K in the former case compared to $\langle \sigma_{T_{eff}} \rangle = 100$ K in the latter case.

5.2 Strömgren colour-T_{eff} calibrations

In addition to the SED fitting, we also derived T_{eff}, R, and L values using Strömgren colour–T_{eff} calibrations for those 537 stars with available Strömgren indices. As in the SED fitting analysis, we opted not to de-redden the colour indices prior to applying the calibrations.

Out of the 537 stars with available Strömgren indices, 32 are identified as Ap stars; in these cases, we applied the calibrations published by Stepień ([1994](#)). These calibrations include bolometric corrections (BCs), which were used along with the available Johnson V magnitudes and distances to derive L and R. For the remaining stars not identified as Ap, we used the calibrations incorporated into the UVBYBETA IDL routine (Moon & Dworetsky [1985](#)). The R and L values were then derived using the same method
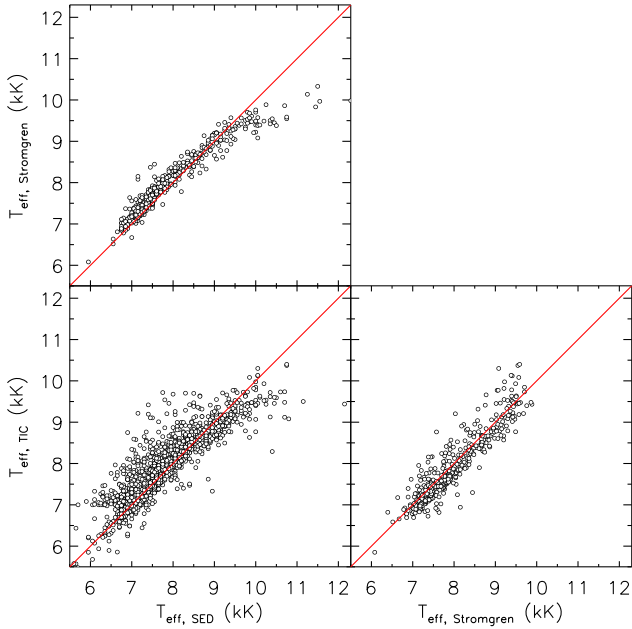
Figure 8. Comparisons between T_{eff} values derived using three methods: $T_{eff, TIC}$ are obtained from the *TESS* Input Catalogue, $T_{eff, Strömgren}$ are derived from a Strömgren colour-T_{eff} calibration, and $T_{eff, SED}$ are derived by fitting synthetic SEDs to various photometric measurements, depending on their availability.

as was applied to the Ap stars where the BCs were calculated from the calibration published by Flower (1996).

The adopted T_{eff}, R, and L values associated with the stars in our sample have been derived using five methods: (i) a spectroscopic-based analysis (Stassun et al. 2018) (12 stars), (ii) SED modelling (1889 stars), (iii) Strömgren colour-T_{eff} calibrations (5 stars) (iv) $(V − K_S) − T_{eff}$ calibrations (41 stars), and (v) a $(V − B) − T_{eff}$ calibration (8 stars). For each star, the method that was used to obtain the final parameters was prioritized based on the order in which they are listed above. In Fig. 8, we compare the first three of these methods for those stars for which multiple methods could be applied. It is evident that, in general, the T_{eff} values derived from the SED modelling and the Strömgren colour-T_{eff} calibration are in agreement with the values listed in the TIC that were derived from $(V − K_S) − T_{eff}$ calibrations. Comparisons between $T_{eff, Strömgren}$ and $T_{eff, SED}$ yield a median absolute deviation of 150 K while comparing $T_{eff, Strömgren}$ and $T_{eff, TIC}$ yields a slightly higher value of 210 K.

5.3 Hertzsprung–Russell diagram

The masses of the stars in our sample were computed by comparing their positions on the HRD with several non-rotating grids of model evolutionary tracks. For stars having masses $< 3.5 M_\odot$, we used the dense grid computed by Mowlavi et al. (2012), which has mass intervals of 0.1 $M_\odot$. For the small number of more massive stars in the sample, we used the grid computed by Ekström et al. (2012), which has larger mass intervals of $0.1 − 2 M_\odot$ for the models with $M \leq 15 M_\odot$. The derivation of the masses and their uncertainties was carried out using the method described by Sikora et al. (2019b).

In Fig. 9 we show the Hertzsprung–Russell diagram (HRD) generated using the sample's derived T_{eff} and L values. These are plotted along with the grid of model evolutionary tracks for solar metallicity, non-rotating stars published by Ekström et al. (2012).
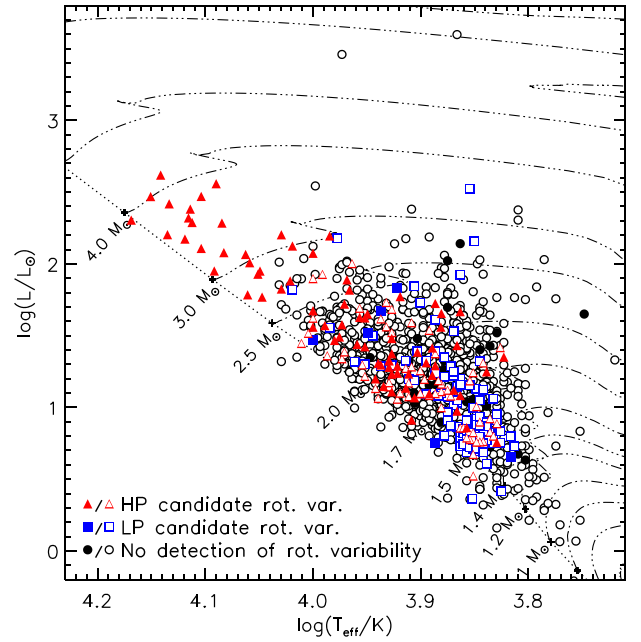

Figure 9. HRD associated with the A-type stars that have been observed with *TESS* in sectors 1–4. The different symbols correspond to high-probability (HP) and low-probability (LP) candidate rotational variables (red triangles and blue squares, respectively); black circles correspond to the rest of the sample (i.e. those stars for which variability consistent with rotational modulation was not detected). Filled symbols correspond to Ap stars; open symbols correspond to stars not identified as Ap.
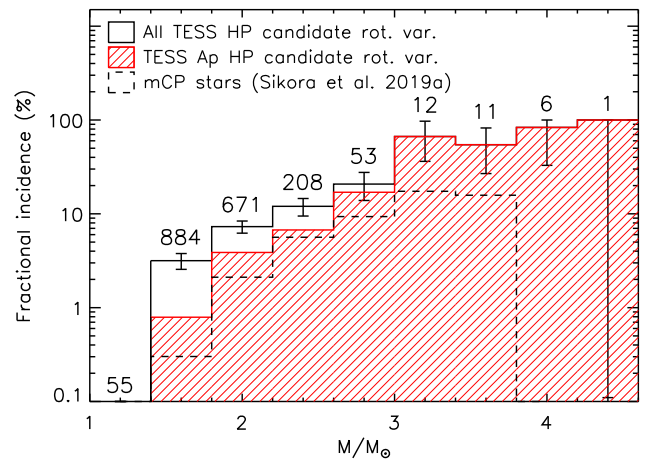

Figure 10. Incidence rate of high-probability (HP) candidate rotational variables as a function of mass where the masses are computed using the derived T_{eff} and L values for the total sample (solid black) and subsample of Ap stars (red hatched). The dashed black line corresponds to the incidence rate of known mCP stars within 100 pc Sikora et al. (2019b). The numbers indicate the total number of stars contained in each bin.

It is evident that the sample roughly spans the entirety of the MS for those stars having $1.4 \lesssim M/M_\odot \lesssim 3$. Based on the HRD, the sample appears to include a small number of post-MS stars, which is consistent with the fact that 212 of the stars in the sample have luminosity classes of II or III. The incidence of the high-probability candidate rotational variable stars as a function of mass is shown in Fig. 10. In Table 2, we list the derived fundamental parameters (T_{eff},

Table 2. Fundamental parameters associated with the 134 identified high probability candidate rotational variables. Columns (1) through (7) list the TIC identifiers, distances (*d*), effective temperatures listed in the TIC ($T_{\mathrm{eff, TIC}}$), effective temperatures ($T_{\mathrm{eff, SED}}$), luminosities (log $L_{\mathrm{SED}}/L_\odot$), and radii (R_{SED}) derived through the SED fitting analysis, and the masses (*M*) derived from comparisons with evolutionary models. The full table appears only in the electronic version of the paper.

TIC	d (pc)	$T_{\mathrm{eff, TIC}}$ (K)	$T_{\mathrm{eff, SED}}$ (K)	log ($L_{\mathrm{SED}}/L_\odot$)	R_{SED} ($R_\odot$)	M_{SED} ($M_\odot$)
(1)	(2)	(3)	(4)	(5)	(6)	(7)
7624182	461 ± 7	8666 ± 229	8450 ± 200	1.68 ± 0.04	3.24 ± 0.15	2.42 ± 0.15
7780491	218 ± 2	8030 ± 220	7700 ± 100	1.29 ± 0.01	2.48 ± 0.05	1.96 ± 0.12
10863314	256 ± 5	8968 ± 234	9050 ± 100	1.69 ± 0.02	2.85 ± 0.08	2.45 ± 0.14
12359289	672 ± 31		12300 ± 250	2.56 ± 0.07	4.19 ± 0.28	3.95 ± 0.20
12393823	226 ± 5	9433 ± 241	10250 ± 100	1.45 ± 0.03	1.68 ± 0.05	2.27 ± 0.09
24186142	272 ± 6		11200 ± 150	1.95 ± 0.04	2.51 ± 0.08	2.94 ± 0.18
24225890	390 ± 8	7163 ± 207	7300 ± 100	1.08 ± 0.02	2.18 ± 0.06	1.75 ± 0.12
27985664	872 ± 75		11550 ± 200	2.07 ± 0.10	2.69 ± 0.27	3.12 ± 0.20
29432990	224 ± 4	7115 ± 207	6750 ± 100	0.89 ± 0.02	2.03 ± 0.07	1.58 ± 0.11
29666185	123 ± 1	7975 ± 219	8200 ± 100	1.27 ± 0.02	2.14 ± 0.03	1.97 ± 0.13
29755072	232 ± 4	8292 ± 224	7800 ± 100	1.54 ± 0.03	3.21 ± 0.09	2.23 ± 0.16
29781099	204 ± 1	8362 ± 225	8100 ± 100	1.28 ± 0.02	2.22 ± 0.05	1.97 ± 0.12
32035258	160 ± 2		13650 ± 200	2.20 ± 0.03	2.26 ± 0.06	3.57 ± 0.14
38586082	126 ± 7	8669 ± 229	9050 ± 100	1.63 ± 0.05	2.65 ± 0.19	2.38 ± 0.14
41259805	243 ± 2	8034 ± 220	8050 ± 100	1.07 ± 0.01	1.76 ± 0.03	1.79 ± 0.11
42055368	174 ± 1	7362 ± 210	7600 ± 100	1.11 ± 0.01	2.07 ± 0.06	1.79 ± 0.11
44627561	408 ± 11	6451 ± 198	6700 ± 100	1.42 ± 0.03	3.79 ± 0.18	1.94 ± 0.15
44678216	93.6 ± 1.9	12503 ± 87	13000 ± 350	2.38 ± 0.04	3.06 ± 0.15	3.70 ± 0.16
44889961	442 ± 8	8823 ± 232	8150 ± 100	1.23 ± 0.02	2.07 ± 0.07	1.93 ± 0.12
52368859	787 ± 26	9076 ± 235	9300 ± 100	1.89 ± 0.04	3.39 ± 0.14	2.72 ± 0.16

log L, M, and R) associated with the 134 high-probability candidate rotational variable stars in our sample.

6 TARGETS OF PARTICULAR INTEREST

As discussed in Section 4, we identified 134 high-probability candidate rotational variables. The *TESS* light curves associated with these targets all exhibit low-frequency peaks in their LS periodograms that are accompanied by at least one harmonic. Here, we discuss some of those targets in our sample which are particularly noteworthy.

6.1 Candidate δ Scuti and roAp stars

Fourteen of the 134 rotational variable candidates are found to exhibit high-frequency peaks in the range $10 \lesssim f \lesssim 65 \, \mathrm{d}^{-1}$ which are associated with δ Scuti pulsators (e.g. Breger 2000; Holdsworth et al. 2014; Bowman & Kurtz 2018) in addition to the low-frequency peaks believed to be associated with rotation. Aside from these periodogram features, no other statistically significant peaks were detected. Only one of the 14 stars (TIC 38586082) has been identified as a δ Scuti pulsator in the literature. Little information is available for the other 13 new candidate δ Scuti stars.

HD 27463 (TIC 38586082) is an ApEuCr(Sr) star (Houk & Cowley 1975) for which a number of photometrically determined rotation periods have been reported (Manfroid & Renson 1981; Mathys & Manfroid 1985). The δ Scuti pulsations were recently discovered by Cunha et al. (submitted) using the same *TESS* light curves analysed in our study. No magnetic field measurements were found in the literature. Anomalous Δa measurements of 26 ± 6 mmag and 28 mmag published by Vogt et al. (1998) and Paunzen & Maitzen (2005), respectively, support the star's Ap classification. Speckle interferometry has been used to detect a companion with a separation of $0.3 \pm 0.4''$ that is dimmer than the

primary component by 0.9 mag in the Strömgren *y* filter (Hartkopf, Tokovinin & Mason 2012). It is plausible that the δ Scuti pulsation peaks are associated with this dimmer companion rather than the Ap star itself. A detailed photometric and spectroscopic analysis of HD 27463 is presented by Khalack et al. (submitted).

In addition to the δ Scuti stars, our sample of high-probability candidate rotational variable stars also contains seven previously discovered roAp stars (TIC 41259805, TIC 211404370, TIC 237336864, TIC 326185137, TIC 340006157, TIC 431380369, and TIC 350146296), and one new candidate roAp star (TIC 259587315).

HD 30849 (TIC 259587315) is a well-known ApSrCrEu star with a reported rotation period of ∼16 d based on Strömgren light curves (Renson 1979; Hensberge et al. 1981). We infer a shorter rotation period of 8.105(6) d based on the *TESS* light curve. Martinez & Kurtz (1994) observed this star twice over time spans ∼1 hr; no high-overtone pulsations typical of roAp stars were detected. Based on the *TESS* light curve, we detect several peaks at frequencies of 78.1 d^{-1}, 80.1 d^{-1}, and 82.1 d^{-1} with respective amplitudes of 0.072 mmag, 0.098 mmag, and 0.118 mmag, which suggest that HD 30849 is likely a roAp star.

6.2 Am stars

Three Am stars were identified as being high-probability candidate rotational variables based on our analysis of their *TESS* light curves (TIC 29781099, TIC 42055368, and TIC 396696863). All three targets are listed in the Catalogue of Ap, HgMn, and Am stars compiled by Renson & Manfroid (2009); however, no definitive information could be found in the literature regarding photometric variability, binarity, or chemical peculiarities. All three light curves and periodograms are shown in Fig. 11 (electronic version) of the electronic version of the paper.

The long rotation periods associated with Am stars, which allow for the formation of these stars' defining chemical peculiarities, are believed to be the result of tidal interactions (Abt 1961). This is consistent with the fact that Am stars are commonly found in short period binary systems (e.g. Carquillat & Prieur 2007). Therefore, it is plausible that the periods identified in the *TESS* light curves may be associated with orbital motions. In this case, large radial velocity variations are expected; spectroscopic monitoring of these targets will need to be carried out in order to determine whether these targets are binaries, and that the observed low-frequency harmonics represent the orbital period.

7 DISCUSSION & CONCLUSIONS

We have identified 134 high-probability candidate rotational variable stars based on 2-min cadence *TESS* light curves among a sample of 1962 A-type stars. More than half of these 134 stars (76 of 134) are identified in the literature as Ap stars, which are expected to exhibit photometric rotational modulation (e.g. Adelman, Dukes & Pyper 1992; Catalano, Leone & Kroll 1998; Samus' et al. 2017; Netopil et al. 2017). Our sample of 1962 A-type stars includes 20 Ap stars for which we did not detect low-frequency variability in their *TESS* light curves. These stars are relatively dim compared to the Ap stars for which low-frequency variability was detected: 75 per cent of the variable Ap stars in our sample have brighter V magnitudes than the median magnitude ($V = 9.5$ mag) of the 20 non-variable Ap stars. The dimmest variable Ap stars in our sample having $V > 9.5$ mag are found to have $\Delta T_{\max} > 0.3$ mmag; therefore, it is likely that any of the dim, apparently non-variable Ap stars that exhibit photometric amplitudes < 0.3 mmag fall below our detection threshold. That being said, less than 10 per cent of the variable Ap stars have $\Delta T_{\max} < 0.3$ mmag, which suggests that only a small number of the 20 non-variable Ap likely have $\Delta T_{\max}$ below this limit.

A significant number of Ap stars are known to have very long rotation periods $\gg 1$ yr (e.g. Landstreet & Mathys 2000; Mathys 2015; Bychkov, Bychkova & Madej 2016; Mathys et al. 2016). It is possible that several of the 20 apparently non-variable Ap stars are variable over timescales that significantly exceed the $28 - 56$ d temporal baseline of the *TESS* light curves used in this study. Alternatively, assuming that these Ap stars host strong, organized magnetic fields similar to other Ap stars and that they have $P_{\rm rot} \lesssim 14$ d, the lack of low-frequency variability may either be indicative of the geometry and structure of the magnetic field or simply be due to the fact that $i = 0°$. The Oblique Rotator Model (ORM, Stibbs 1950; Preston 1967) predicts that no longitudinal magnetic field variability will be observed in the case in which (i) the magnetic field is axially symmetric and (ii) the axis of symmetry is parallel to the star's axis of rotation. Since the chemical spots which produce the non-uniform surface brightness distributions are known to be correlated with the magnetic field topology (Kochukhov et al. 2004; Silvester, Kochukhov & Wade 2014; Kochukhov et al. 2017), the star's rotation might lead to weak or absent photometric variability in this specific case.

The 134 high-probability candidate rotational variable stars includes 58 A-type stars that are not identified as Ap based on the spectral types obtained from SIMBAD. We find that these stars' light curves are statistically distinct from the 76 identified candidate rotational variable Ap stars both in terms of the distribution of inferred $P_{\rm rot}$ values and in terms of their distribution of photometric amplitudes, $\Delta T_{\max}$. The (presumably) non-Ap stars tend to exhibit much lower values of $\Delta T_{\max}$ than the Ap stars: ≈ 60 per cent of the non-Ap stars have $\Delta T_{\max} \lesssim 1$ mmag compared to <7 per cent of the Ap stars. The distribution of rotation periods inferred for the Ap stars in our sample is found to be in agreement with that reported by Sikora et al. (2019a) for nearby mCP stars. The non-Ap stars in our sample tend to rotate more rapidly based on the inferred rotation periods. This is to be expected from normal (i.e. non-chemically peculiar) A-type stars; nevertheless, comparing with published distributions of A star $v \sin i$ values (Abt & Morrell 1995; Zorec & Royer 2012) suggests that the inferred $P_{\rm rot}$ values are unusually long for non-CP A stars. Including those non-CP stars identified in our sample as low-probability candidate rotational variables reduces the discrepancy but does not change the conclusion that the distribution of periods is inconsistent with that of non-CP A-type stars.

The photometric variability associated with Ap stars is well understood to be associated with strong, organized, and stable magnetic fields that are visible at the stellar surface. The origin of the identified rotational variability associated with the non-Ap star light curves, however, is unclear. It is plausible that the A stars are not intrinsically variable but that the observed variability is related to late-type binary companions or late-type background stars. A similar explanation for the origin of a number of flares in *Kepler* light curves of A-type stars was presented by Pedersen et al. (2017). This is a distinct possibility especially considering the relatively large 21″ pixel size of the *TESS* CCDs (Sullivan et al. 2015) (cf. *Kepler*'s 4″ pixel size, Koch et al. 2010).

Assuming that the identified rotational variability of the non-Ap stars is intrinsic to the A stars themselves, it cannot be excluded that the variability is caused by the same mechanism that is responsible for the formation of dynamic, low-contrast chemical spots on HgMn stars. No convincing evidence of a surface magnetism has been found for HgMn stars (e.g. Shorlin et al. 2002; Wade et al. 2006; Makaganiuk et al. 2010). Consequently, it was suggested (Kochukhov et al. 2007) that their spots are not linked to magnetic fields but are formed under the influence of hydrodynamic instabilities associated with the build-up of chemical anomalies by radiative diffusion. Numerical simulations (Alecian, Stift & Dorfi 2011; Deal, Richard & Vauclair 2016) demonstrate possibility of such instabilities for both late-B and A-type stellar parameter ranges, though it is not clear at the moment what governs the horizontal spatial scales of these structures. A comparison of the photometric behaviour of known HgMn stars with the present non-Ap sample is necessary to assess their similarities and differences. Furthermore, detailed abundance analysis of newly discovered rotational variables is required to ascertain their status as chemically normal stars. As noted above, the rotation periods associated with our sample of non-Ap stars appear to be unusually long for non-CP A stars, which suggests that this subsample may include unrecognized chemically peculiar stars with moderate abundance anomalies (e.g. marginal Am and HgMn stars).

The detection of ultra-weak magnetic fields with strengths $\lesssim 1$ G on a small but growing number of non-Ap stars such as Vega (Lignières et al. 2009; Petit et al. 2011; Blazère, Neiner & Petit 2016) has led to speculation that such fields may be widespread amongst the population of non-Ap stars (e.g. Petit et al. 2011). Given that (i) chemical and/or temperature spots have been detected on the surface of Vega (Böhm et al. 2015) and that (ii) these spots exhibit a similarly complex topology to that of the detected magnetic field (Petit et al. 2010, 2017), it is plausible that the non-Ap candidate rotational variables identified in our study also host ultra-weak fields, which are responsible for the observed variability. This explanation has been put forth in response to the discovery by Balona (2013) that ~ 40 per cent of A-type stars observed with *Kepler* appear to exhibit

rotational variability. Braithwaite & Cantiello (2013) have proposed that such ultra-weak fields may be so-called *failed fossils* – weak fields having a similar origin to the fossil fields that are widely believed to be associated with mCP stars (Cowling 1945). The strengths of failed fossil magnetic fields are predicted to decrease as the star evolves across the MS and have strengths that are anti-correlated with P_{rot}. While Braithwaite & Cantiello (2013) do not provide any predictions regarding photometric variability, the authors note that changes in a failed fossil (and presumably, any chemical spots that may be associated with the field) should not be detectable. Evidence of AMod was found in the light curves of 10 of the 48 high-probability candidate rotational variable non-CP MS stars in our sample, which could be indicative of evolving surface spot morphologies. Assuming that the detected AMod is intrinsic to the A stars and not the result of contamination from binary companions or background stars, these detections would be inconsistent with the failed fossil model.

Cantiello & Braithwaite (2019) explored an alternative explanation for the origin of ultra-weak fields in A- and late B-type stars, which involves dynamo fields that are generated near the stellar surface. The authors suggest that (i) all rapidly rotating A- and B-type stars possess sub-surface H and He convection zones where turbulent dynamo may generate magnetic fields and that (ii) these fields are associated with bright temperature spots similar to those predicted to exist on more massive stars (Cantiello & Braithwaite 2011). A rotation-activity connection is known to be a key feature of any type of dynamo-powered magnetic field and associated surface activity. According to Cantiello & Braithwaite (2019), the dynamo action requires stellar rotation with periods of $0.5 - 1$ d for a dwarf star with parameters similar to Vega. Among the 48 MS non-CP stars in our sample only 20 have $P_{rot} \leq 1.5$ d and the rest are slower rotators with P_{rot} up to 7.5 d for which no dynamo action is anticipated. Moreover, we do not observe a clear anticorrelation between P_{rot} and ΔT_{max}, which is expected within the framework of any dynamo hypothesis. As noted above, we do find evidence of AMod in the light curves of 10 of the 48 MS non-CP stars. These 10 stars have inferred rotation periods ranging from 0.5 to 4.6 d and all but 4 have $P_{rot} \leq 1.5$ d. We also note that we did not find evidence of AMod for an additional 17 of the MS non-CP stars with $P_{rot} \leq 1.5$ d.

It is likely that in order to better understand the origin of the variability associated with the non-Ap stars identified in our sample as being rotational modulation we will need to obtain high-resolution spectroscopic measurements. The measurement of chemical abundancies in the atmosphere's of these stars is of particular interest as it may confirm our suspicion that some of the stars in our sample are at least weakly chemically peculiar. Detecting spectroscopic variability or placing constraints on the strength of such variability would also be useful in this regard. We also note that combining the *TESS* light curves with multi-colour long-term monitoring, such as that provided by the *BRITE*-Constellation mission (Weiss 2008), may provide insight into the puzzling results presented here.

REFERENCES

Abt H. A., 1961, ApJS, 6, 37
Abt H. A., Morrell N. I., 1995, ApJS, 99, 135
Adelman S. J., Dukes R. J., Jr, Pyper D. M., 1992, AJ, 104, 314
Adelman S. J., Gulliver A. F., Kochukhov O. P., Ryabchikova T. A., 2002, ApJ, 575, 449
Alecian G., Gebran M., Auvergne M., Richard O., Samadi R., Weiss W. W., Baglin A., 2009, A&A, 506, 69
Alecian G., Stift M. J., Dorfi E. A., 2011, MNRAS, 418, 986
Astraatmadja T. L., Bailer-Jones C. A. L., 2016, ApJ, 833, 1
Aurière M. et al., 2007, A&A, 475, 1053
Aurière M. et al., 2010, A&A, 523, A40
Auvergne M., Bodin P., Boisnard L., Buey J., Chaintreuil S., Epstein G., Jouret M., 2009, A&A, 506, 411
Babcock H. W., 1960, ApJ, 132, 521
Babcock H. W., Burd S., 1952, ApJ, 116, 8
Bagnulo S., Fossati L., Landstreet J. D., Izzo C., 2015, A&A, 583, 1
Bailer-Jones C. A. L., Rybizki J., Fouesneau M., Mantelet G., Andrae R., 2018, AJ, 156, 58
Balona L. A. et al., 2011, MNRAS, 413, 2403
Balona L. A., 2011, MNRAS, 415, 1691
Balona L. A., 2012, MNRAS, 423, 3420
Balona L. A., 2013, MNRAS, 431, 2240
Balona L. A., 2014, in Mathys G., Griffin E., Kochukhov O., Monier R., Wahlgren G., eds, Puting. A Stars into Context Evololution, Environment, and Related Stars Variability of Kepler A- and B-type stars Starspots on A-type stars. Pero, Moscow, Russia, p. 415
Berdyugina S. V., 2005, Liv. Rev. Sol. Phys., 2, 1
Bessell M., Murphy S., 2012, PASP, 124, 140
Bessell M. S., 2011, PASP, 123, 1442
Blazère A., Petit P., Lignières F., Aurière M., Ballot J., Böhm T., Folsom C. P., Gaurat M., 2016, A&A, 586, A97
Blazère A., Neiner C., Petit P., 2016, MNRAS, 459, L81
Böhm T. et al., 2015, A&A, 577, A64
Borra E. F., Landstreet J. D., 1980, ApJS, 42, 421
Borucki W. J. et al., 2010, Science, 327, 977
Bowman D. M., Kurtz D. W., 2018, MNRAS, 476, 3169
Bowman D. M., Kurtz D. W., Breger M., Murphy S. J., Holdsworth D. L., 2016, MNRAS, 460, 1970
Bowman D. M., Buysschaert B., Neiner C., Pápics P. I., Oksala M. E., Aerts C., 2018, A&A, 616, A77
Braithwaite J., Cantiello M., 2013, MNRAS, 428, 2789

Breger M., Montgomery M., eds, 2000, Delta Scuti and Related Stars Vol. 210 of Astronomical Society of the Pacific Conference Series, δ Scuti stars (Review), Astron. Soc. Pac., San Francisco, CA, p. 3

Briquet M., Korhonen H., González J. F., Hubrig S., Hackman T., 2010, A&A, 511, A71

Buysschaert B. et al., 2018, MNRAS, 478, 2777

Bychkov V. D., Bychkova L. V., Madej J., 2016, MNRAS, 455, 2567

Cameron A. C., Donati P. J., Semel M., 2002, MNRAS, 330, 699

Cantiello M., Braithwaite J., 2011, A&A, 534, A140

Cantiello M., Braithwaite J., 2019, preprint (arXiv:1904.02161)

Carquillat J., Prieur J., 2007, MNRAS, 380, 1064

Casagrande L., Flynn C., Bessell M., 2008, MNRAS, 389, 585

Castelli F., Kurucz R. L., 2003, in Piskunov N., Weiss W. W., Gray D. F., eds, Modelling of Stellar Atmospheres Vol. 210 of IAU Symposium, New Grids of ATLAS9 Model Atmospheres, Astron. Soc. Pac., San Francisco, CA. p. A20

Catalano F. A., Leone F., Kroll R., 1998, A&AS, 129, 463

Cohen M., Wheaton W. A., Megeath S. T., 2003, AJ, 126, 1090

Cousins A. W. J., Caldwell J. A. R., Menzies J. W., 1989, IBVS, 3412, 1

Cowling T. G., 1945, MNRAS, 105, 166

David-Uraz A. et al., 2019, MNRAS, 487, 304

De Cat P., Aerts C., 2002, A&A, 393, 965

Deal M., Richard O., Vauclair S., 2016, A&A, 589, A140

Degroote P. et al., 2011, A&A, 536, A82

Díaz-Cordovés J., Claret A., Gimenez A., 1995, A&AS, 110, 329

Ducati J. R., 2002, VizieR Online Data Catalog, 2237

Eker Z., 1994, ApJ, 420, 373

Ekström S. et al., 2012, A&A, 537, A146

Ermolli I., Criscuoli S., Centrone M., Giorgi F., Penza V., 2007, A&A, 465, 305

ESAed., 1997, The HIPPARCOS and TYCHO catalogues. Astrometric and photometric star catalogues derived from the ESA HIPPARCOS Space Astrometry Mission, Vol. 1200, ESA Special Publications, Noordwijk, The Netherlands

Flower P. J., 1996, ApJ, 469, 355

Folsom C. P., Kochukhov O., Wade G. A., Silvester J., Bagnulo S., 2010, MNRAS, 407, 2383

Gaia Collaboration, Prusti T., Bruijne J. H. J. D., Brown A. G. A., Vallenari A., Babusiaux C., 2016, A&A, 595, 1

Ghazaryan S., Alecian G., 2016, MNRAS, 460, 1912

Gontcharov G. A., Mosenkov A. V., 2017, MNRAS, 472, 3805

Gray D., 2005, The Observation and Analysis of Stellar Photospheres. Cambridge Univ. Press, Cambridge

Grevesse N., Sauval A. J., 1998, Space Sci. Rev., 85, 161

Hartkopf W. I., Tokovinin A., Mason B. D., 2012, AJ, 143, 42

Hauck B., Mermilliod M., 1997, VizieR Online Data Catalog, 2215

Henry G. W., Fekel F. C., 2003, AJ, 126, 3058

Hensberge H. et al., 1981, A&AS, 46, 151

Hodgson J. A., Krichbaum T. P., Marscher A. P., Jorstad S. G., Rani B., Bach U., 2017, A&A, 597, A80

Holdsworth D. L. et al., 2014, MNRAS, 439, 2078

Holl B. et al., 2018, A&A, 618, A30

Houk N., Cowley A. P., 1975, University of Michigan Catalogue of two-dimensional spectral types for the HD stars. Volume I. Declinations -90 to -53, Department of Astronomy, University of Michigan, Ann Arbor, MI

Howell S. B. et al., 2014, PASP, 126, 398

Huang Y., Liu X., Yuan H., Xiang M., Chen B., Zhang H., 2015, MNRAS, 454, 2863

Jenkins J. M. et al., 2016, in Chiozzi G., Guzman J. C., eds, The TESS science processing operations center, SPIE, San Francisco, CA, p. 99133E–1

Kochukhov O. et al., 2013, A&A, 554, A61

Kochukhov O., Sudnik N., 2013, A&A, 554, A93

Kochukhov O., Bagnulo S., Wade G. a., Sangalli L., Piskunov N. E., Landstreet J. D., Petit P., Sigut T. A. A., 2004, A&A, 414, 613

Kochukhov O., Piskunov N., Sachkov M., Kudryavtsev D., 2005, A&A, 439, 1093

Kochukhov O., Adelman S. J., Gulliver A. F., Piskunov N., 2007, Nature Phys., 3, 526

Kochukhov O., Silvester J., Bailey J. D., Landstreet J. D., Wade G. A., 2017, A&A, 605, A13

Koch D. G. et al., 2010, ApJ, 713, L79

Korhonen H. et al., 2013, A&A, 553, A27

Krtička J., Mikulášek Z., Zverko J., Žižńovský J., 2007, A&A, 470, 1089

Krtička J., Mikulášek Z., Henry G. W., Zverko J., Žižovský J., Skalický J., Zvěrina P., 2009, A&A, 499, 567

Krtička J., Mikulášek Z., Lüftinger T., Jagelka M., 2015, A&A, 576, A82

Kudryavtsev D. O., Romanyuk I. I., Elkin V. G., Paunzen E., 2006, MNRAS, 372, 1804

Landstreet J. D., 1982, ApJ, 258, 639

Landstreet J. D., Mathys G., 2000, A&A, 359, 213

Lignières F., Petit P., Böhm T., Aurière M., 2009, A&A, 500, L41

Lignières F., Petit P., Aurière M., Wade G. A., Böhm T., 2014, Proc. IAU Symp. No. 302 No. 302, The dichotomy between strong and ultra-weak magnetic fields among intermediate-mass stars. Cambridge Univ. Press, Cambridge, p. 338

Lomb N. R., 1976, Astrophys. Space Sci., 263, 835

Makaganiuk V. et al., 2010, A&A, 525, A97

Makaganiuk V. et al., 2012, A&A, 539, A142

Manfroid J., Renson P., 1981, IBVS, 2004, 1

Martinez P., Kurtz D. W., 1994, MNRAS, 271, 129

Mathys G., 2015, Phys. Evol. Magn. Relat. Stars (Very) Slow Rotation of Magnetic Ap Stars, Astron. Soc. Pac. San Francisco, CA, p. 3

Mathys G., Manfroid J., 1985, A&AS, 60, 17

Mathys G., Romanyuk I. I., Kudryavtsev D. O., Landstreet J. D., Pyper D. M., Adelman S. J., 2016, A&A, 586, 1

Matson R. A., Gies D. R., Guo Z., Williams S. J., 2017, AJ, 154, 216

Montgomery M. H., O'Donoghue D., 1999, Delta Scuti Star Newslett., 13, 28

Moon T. T., Dworetsky M. M., 1985, MNRAS, 217, 305

Morel T. et al., 2011, A&A, 533, A4

Mowlavi N., Eggenberger P., Meynet G., Ekström S., Georgy C., Maeder A., Charbonnel C., Eyer L., 2012, A&A, 541, A41

Netopil M., Paunzen E., Hümmerich S., Bernhard K., 2017, MNRAS, 468, 2745

Oelkers R. J. et al., 2018, AJ, 155, 39

Papaloizou J., Pringle J. E., 1978, MNRAS, 182, 423

Paunzen E., Maitzen H. M., 2005, A&A, 441, 631

Paunzen E., Fröhlich H., Netopil M., Weiss W. W., Lüftinger T., 2015, A&A, 574, A57

Pedersen M. G., Antoci V., Korhonen H., White T. R., Lehtinen J., Nikbakhsh S., Viuho J., 2017, MNRAS, 466, 3060

Petit P. et al., 2010, A&A, 523, 1

Petit P. et al., 2011, A&A, 532, L13

Petit P., Lignières F., Wade G. A., Aurière M., Alina D., Bohm T., Oza A., 2011, Astron. Nachr., 332, 943

Petit P., Hébrard E. M., Böhm T., Folsom C. P., Lignières F., 2017, MNRAS, 472, L30

Pourbaix D., Tokovinin A. A., Batten A. H., Fekel F. C., Hartkopf W. I., 2004, A&A, 424, 727

Press W., 2007, Numerical Recipes 3rd Edition: The Art of Scientific Computing. Cambridge Univ. Press, Cambridge

Preston G. W., 1967, ApJ, 150, 547

Renson P., 1979, A&A, 77, 366

Renson P., Manfroid J., 2009, A&A, 498, 961

Ricker G. R. et al., 2015, J. Astron. Telesc. Instrum., Syst., 1, 1

Rufener F., Nicolet B., 1988, A&A, 206, 357

Saio H., Kurtz D. W., Murphy S. J., Antoci V. L., Lee U., 2018, MNRAS, 474, 2774

Samus' N. N., Kazarovets E. V., Durlevich O. V., Kireeva N. N., Pastukhova E. N., 2017, Astron. Rep., 61, 80

Scargle J. D., 1982, ApJ, 263, 835

Shorlin S. L. S., Wade G. A., Donati J.-F., Landstreet J. D., Petit P., Sigut T. A. A., Strasser S., 2002, A&A, 392, 637

Sikora J., Wade G. A., Power J., Neiner C., 2019a, MNRAS, 483, 2300
Sikora J., Wade G. A., Power J., Neiner C., 2019b, MNRAS, 483, 3127
Silvester J., Kochukhov O., Wade G. A., 2014, MNRAS, 444, 1442
Smalley B. et al., 2014, A&A, 564, A69
Stassun K. G. et al., 2018, AJ, 156, 102
Stepień K., 1994, in Zverko J., Ziznovsky J., eds, Chemically Peculiar and
    Magnetic Stars Properties and position of CP2 stars on the HR diagram.
    Tatranska Lomnica, Slovak Republic, p. 8
Stibbs D. W. N., 1950, MNRAS, 110, 395
Sullivan P. W. et al., 2015, ApJ, 809, 77
van Leeuwen F., 2007, A&A, 474, 653
Van Reeth T., Tkachenko A., Aerts C., 2016, A&A, 593, A120
Vogt N., Kerschbaum F., Maitzen H., Faundez-Abans M., 1998, A&AS,
    130, 455
Wade G. A. et al., 2006, A&A, 451, 293
Waelkens C., 1991, A&A, 246, 453
Weiss W. W., 2008, Commun. Asteroseismol., 152, 6
Wolff S. C., 1968, PASP, 80, 281
Wolff S. C., 1975, ApJ, 202, 127
Zorec J., Royer F., 2012, A&A, 537, A120

SUPPORTING INFORMATION

Supplementary data are available at *MNRAS* online.

Table 1. Parameters associated with the 134 identified high probability candidate rotational variables.

Table 2. Fundamental parameters associated with the 134 identified high probability candidate rotational variables.

Figure 11. Examples of TESS light curves associated with Am stars that are found to exhibit variability that is consistent with a rotational origin. *Left:* Subsamples of the full light curves. *Right:* The Lomb-Scargle periodograms derived from the light curves. The rotational frequencies are apparent along with the rst harmonic. The spectral window function is shown in the top right.

Please note: Oxford University Press is not responsible for the content or functionality of any supporting materials supplied by the authors. Any queries (other than missing material) should be directed to the corresponding author for the article.

This paper has been typeset from a TEX/LATEX file prepared by the author.